

Published in final edited form as:

*Magn Reson Imaging*. 2010 November ; 28(9): 1299–1305. doi:10.1016/j.mri.2010.06.003.

## Interrelationships between 3T MRI derived cortical and trabecular bone structure parameters and quantitative computed tomography derived bone mineral density

AS Issever, MD<sup>1,2</sup>, TM Link, MD<sup>1</sup>, D Newitt, PhD<sup>1</sup>, T Munoz, MD<sup>1</sup>, and S Majumdar, PhD<sup>1</sup>

<sup>1</sup>Musculoskeletal and Quantitative Imaging Research Group, Department of Radiology and Biomedical Imaging, University of California, San Francisco, China Basin, 185 Berry Street, Lobby 6, Suite 350, San Francisco, California 94107, USA

<sup>2</sup>Department of Radiology, Charité Campus Mitte Universitätsmedizin Berlin, Charitéplatz 1, 10115 Berlin, Germany

### Abstract

Recently 3T magnetic resonance imaging (MRI) has been introduced for bone imaging. Through higher signal-to-noise ratios, as compared to 1.5 T MRI, it promises to be a more powerful tool for the assessment of cortical and trabecular bone measures. The goal of our study was to compare MRI derived cortical and trabecular bone measures to quantitative computed tomography (QCT) derived bone mineral density (BMD).

Using 3T MRI in 51 postmenopausal women apparent (app.) measures of bone volume/total volume, trabecular number (Tb.N), trabecular thickness (Tb.Th) and trabecular separation were derived at the distal radius, distal tibia and calcaneus. Cortical thickness (Ct.Th) was calculated at the distal radius and distal tibia. These measures were compared to QCT derived BMD of the spine, hip and radius.

Significant correlations (\* $p < 0.05$ ; \*\* $p < 0.001$ ; \*\*\* $p < 0.0001$ ) were found between spine BMD and MRI derived Ct.Th ( $r_{\text{radius}} = 0.55^*$ ;  $r_{\text{tibia}} = 0.67^{***}$ ) and app. Tb.N ( $r_{\text{radius}} = 0.33^*$ ;  $r_{\text{tibia}} = 0.35^*$ ) at the radius and tibia. Furthermore within the first 10mm at the radius an inverse correlation for cort. thick and app. BV/TV ( $r_{6\text{mm}} = -0.56$ ,  $p < 0.001$ ;  $r_{10\text{mm}} = -0.36$ ,  $p < 0.05$ ) and app. Tb.Th ( $r_{6\text{mm}} = -0.54$ ,  $p < 0.001$ ;  $r_{10\text{mm}} = -0.41$ ,  $p < 0.05$ ) was found..

### Keywords

3T MRI; cortical bone; trabecular bone; osteoporosis

### Introduction

Osteoporosis is a systemic bone disease, characterized by reduced bone strength and a clinically manifested increase of fractures due to low-impact trauma. These fractures, especially at the

© 2010 Elsevier Inc. All rights reserved.

**Corresponding author:** ahi-sema.issever@charite.de, phone: + 49 - 30 - 450 - 627 043, fax: + 49 - 30 - 450 - 527 911.

**Publisher's Disclaimer:** This is a PDF file of an unedited manuscript that has been accepted for publication. As a service to our customers we are providing this early version of the manuscript. The manuscript will undergo copyediting, typesetting, and review of the resulting proof before it is published in its final citable form. Please note that during the production process errors may be discovered which could affect the content, and all legal disclaimers that apply to the journal pertain.

site of the hip are commonly associated with immobilization, a significant decrease in the quality of life and a high mortality rate.

The amount of mineralized bone, assessed as bone mineral density (BMD) is a fundamental determinant of bone strength (1–4). BMD has been shown to account for approximately 60 – 70% of bone strength (5,6). However, mere BMD measurements alone do not provide a sufficient discrimination between patients with and without increased fracture risk (6–8). Thus to assess bone strength and to estimate the fracture risk, basic mechanical principles demand that beyond BMD, the spatial distribution of the material needs to be assessed as well.

The concept of "bone quality" was introduced by the National Institutes of Health Consensus Conference on Osteoporosis in 2001 (5). Bone quality refers to the "sum total of characteristics of the bone that influence the bone's resistance to fracture"(9). Beyond BMD these characteristics include the material composition of bone and its components (collagen, matrix proteins, mineral, water etc.). And furthermore it includes measures of the bones morphology, macro- and microarchitecture as well as dynamic measures such as the rate of bone turnover (10).

For the assessment of BMD, which reflects the material properties of bone, densitometry methods have been established. DXA and QCT are the most frequently applied densitometry measurement methods in clinical practice.

Among the most important parameters reflecting the structural properties of bone, are those measuring trabecular and cortical bone micro- and macrostructure (11). In terms of clinically applicable imaging methods though, it remains a challenge to accurately depict and assess trabecular and cortical bone measures.

For over a decade, the role of MR imaging in the analysis of bone architecture has been investigated using 1.5 T MR systems (12–18). Despite the numerous established applications using 1.5T MR scanners, technical limitations need to be considered when bone analysis is performed. Such limitations include signal-to-noise constraints, restricted spatial in-plane resolution, anisotropic voxels due to slice thicknesses larger than the in-plane dimension, partial volume effects and susceptibility artifacts. With the introduction of 3T MR scanner systems it has been shown that higher-field strengths result in significant higher signal-to-noise ratios, and multiple in vitro studies have been shown that 3T MR derived trabecular and cortical measures reflect, more accurately than 1.5T derived measures, the true structure of bone (19–22).

This current study was performed to (i) demonstrate the feasibility of in vivo 3T MR imaging for the derivation of trabecular and cortical measures at non-weight bearing and weight bearing sites (radius vs. tibia and calcaneus); to (ii) intercorrelate trabecular and cortical measurements and to (iii) assess the relationship of MR derived measurements with volumetric QCT measures of the spine, the hip and the radius.

## Materials and Methods

### Study participants

51 postmenopausal female volunteers participated in our study (mean age 62 years; age range, 44 – 85 years). Known bone metabolic disease conditions such as young idiopathic osteoporosis were considered exclusion criteria for the study, and other disease conditions or drug treatments that may lead to secondary alterations in bone metabolism. All volunteers underwent quantitative computed tomography (QCT) of the spine, the proximal femur, and distal radius and high resolution MRI of the distal radius, the distal tibia and the calcaneus. Imaging of the

distal radius, the distal tibia and calcaneus was performed on the nondominant limb. Furthermore, body height and weight were assessed to compute body mass index (BMI) measures. The institutional review board approved the study and written informed consent was obtained from all volunteers.

### **Volumetric quantitative computed tomography (QCT)**

All examinations were performed with a 16-row multidetector (MD) Spiral CT scanner (Mx8000 IDT, Philips Medical Systems, Best, Netherlands) and a dedicated calibration phantom. After image acquisition commercially available software (Mindways, CA, USA) was used to assess volumetric BMD. Standard, QCT examinations of L1 – L3 and of the proximal femur were performed in all subjects. The subject was positioned supine on the CT scanner table for the scans of the spine and the proximal femur with the calibration phantom located in the table mat in the region of interest. The spine scan was prescribed from the lateral scout and the scan included L1 – L3 vertebrae. The hip scan was prescribed from the AP scout and covered enough volume to include the hip from the top of the head to the lesser trochanter. A standard QCT protocol with 120 kVp, 90 mAs, and a slice thickness and increment of 3 mm was used. Lumbar BMD was determined in oval regions of interest in the anterior  $\frac{3}{4}$  of the trabecular compartment of the L1 – L3 vertebra in an approximately 1 cm thick volume in the center of each vertebra, parallel to both endplates. Femoral BMD was determined in the trabecular compartment of the total proximal femur; after the bone was automatically segmented into the cortical and trabecular compartment, using a threshold-based algorithm provided by the manufacturer. Average 3D BMD values (mg/cm<sup>3</sup>) of the trabecular compartment of L1 – L3 and the proximal femur were computed by using dedicated commercially available software (Mindways Software, Austin, TX, USA).

In addition, a QCT scan of the distal radius was obtained. For the wrist scan, the subject was positioned prone on the table with the arm extended above the head. The wrist was scanned with 80 kVp, 100 mAs at 0.75 seconds rotation time, pitch 0.9, field of view (FOV) 10 cm, and the slice thickness and increment were 2 mm. The wrist scan was prescribed to include the distal endplate. For assessment of radial BMD values in-house IDL (RSI, Boulder, CO, USA) software was used. As the histogram intensity distribution of the QCT images is bimodal, fully automatic threshold-based segmentation was performed to define the trabecular compartment. BMD values (mg/cm<sup>2</sup>) of the trabecular compartment were then computed on a section-by-section basis to ensure comparability with the MR images (see analysis regions and registration of MRI and QCT results section).

### **3T MRI Scan Parameters**

MRI was performed on a 3T Signa scanner (General Electric, Milwaukee, WI, USA) using a transmit/receive quadrature wrist coil (Mayo Foundation for Medical Education and Research, Rochester, MN, USA) for the distal radius and a 4-channel dual-paddle surface array coil (Nova Medical, Wilmington, MA, USA) for the tibia and calcaneus. Custom-built immobilization devices were used to reduce motion artifacts and to provide reproducible subject and coil positioning. Wrist imaging was done with the subject lying prone with their arm held over their head. The coil was mounted to an indexed plate set at a fixed 20 degree angle to the magnet bore and approximately 5 cm from iso-center. This position was found to give a reasonable compromise between subject comfort and signal-to-noise (SNR) loss due to coil rotation and displacement from iso-center. Ankle and foot images were acquired with the subject lying supine with the imaged leg secured in a custom holder.

For the distal radius imaging, a 3-plane localizer was obtained to check positioning and to visualize joint geometry for prescribing an anatomical coronal scout adjusted for coil and wrist rotation relative to the scanner axes. Axial “thick slice” (TS scan: 3D steady state free

precession (SSFP) with 30 degree flip angle; 2 mm slice thickness; 512×512×32 matrix; 1 NEX; 8 cm FOV) and “high resolution” (HR scan: 3D SSFP with 40 degree flip angle; 0.5 mm slice thickness; 512×384×64 matrix; 2 NEX; 8 cm FOV) scans were prescribed on the coronal scout for cortical and trabecular bone quantification.

For the lower leg scans, a large FOV sagittal scout was run initially to check coil positioning and to prescribe 3 plane localizers on the calcaneus and on the distal tibia. Axial TS and HR scans were run on the tibia, similar to those on the radius except that a fully balanced SSFP (bSSFP), flip angle 60 degrees, sequence was used for the tibia HR scan. For the calcaneus only a sagittal HR scan for trabecular structure was run, using the bSSFP sequence with FOV of 10 cm. TE and TR were set automatically by the scanner for all sequences. TR varied from 10.7 ms to 14 ms for the TS scans, from 15.7 to 18.1 ms for the radius and tibia HR scans, and from 11.5 ms to 11.8 ms for the calcaneus scan. TE varied from 3.2 ms to 4.7 ms for all the SSFP scans, and was 6.5 ms for the bSSFP sequence.

All axial scans on the radius and tibia were aligned with the distal end of the scan prescription approximately on the distal endplate, giving coverage in the TS scans of the most distal 5 cm of the bone and in the HR scans of approximately 2.5 cm, allowing for rejection of end slices due to aliasing in the slice direction. The non-balanced SSFP sequence was chosen for TS cortical imaging primarily for the high bone/muscle contrast allowing easier segmentation of the periosteal boundary, and on the radius HR scan to minimize banding artifacts from off resonance effects. The bSSFP sequence was used to maximize SNR in the HR tibia and calcaneus scans where no significant banding artifacts were present.

The entire length of the MRI examination, including positioning, was from 1 to 1.5 hours, depending on whether any HR scans needed to be repeated. Individual scan times were approximately 20 minutes each for the distal radius, distal tibia and calcaneus.

## MRI structural analysis

All images were transferred from the scanner to a Sun workstation (Mountain View, California, USA) for segmentation and quantitative bone analysis using locally written software. Trained experts performed the trabecular ROI definition on the radius, tibia, and calcaneus MR images first using a semi-automated algorithm, and then editing the regions of interest manually. The regions of interest in the radial QCT and MR scans were matched using bone area as a metric in an image registration algorithm. Furthermore, visual coregistration was used to confirm matching ROIs. Cortical thickness (Ct.Th) for the radius and tibia was calculated from the TS images, which showed a clear cortical shell, using endosteal and periosteal surfaces manually defined on each image. The geometric measures were calculated using the 3D direct distance transformation method developed for trabecular structure measurement (23). Following image binarization apparent trabecular structure measures (24) were derived, as previously described in detail by Majumdar et al. (15). The trabecular structure measures had to be defined as apparent (app.) due to lower spatial resolution constraints of the MR images. Thus, app. bone volume/total volume (BV/TV), app. trabecular number (Tb.N), thickness (Tb.Th) and separation (Tb.Sp) were computed. Briefly, the total number of bright pixels contributing to the bone phase in the binarised image relative to the total number of pixels in the ROI was used to compute app. BV/TV. The total numbers of black and white pixel edges that cross a set of parallel rays at a given angle  $\theta$  through the image were counted, and then a measure of the mean intercept length was computed as the ratio between the total area of the bright pixels and half the number of edges. The mean value of the intercept length for all angles provided the width of the bright pixels and was defined as app. Tb.Th. From these measurements, of app. BV/TV and app. Tb.Th, app. Tb.N (area fraction of bright pixels/ app. Tb.Th) and app. Tb.Sp ( $[1/\text{app. Tb.N}] - \text{app. Tb.Th}$ ) were calculated. Reproducibility given as the percent coefficient

of variation is 3.7 to 5.2 for app. BV/TV, 2.5 to 4.1 for app. Tb.N, 2.9 to 3.4 for app. Tb.Th and 4.0 to 8.3 for app. Tb.Sp (25). For the tibia and calcaneus analysis the images were first corrected for surface coil sensitivity inhomogeneities using a low-pass filter based algorithm, modified for trabecular bone images.

### Analysis regions and registration of MRI and QCT results

A distal endplate reference position was determined for each TS and HR acquisition by visual inspection of the MR images. As all MRI and QCT scans were done in the axial plane, and since no in-plane regional analysis was done, a simple 1D registration (axial shifting) was used to determine matching regions between the MRI and the QCT images. The relative axial shift was determined by a fully automatic routine comparing plots of trabecular area on each slice with respect to position, giving the endplate reference for the QCT images corresponding to that determined manually for the MRI images. For the HR scans the analysis region began 6mm (radius) or 12 mm (tibia) proximal from the endplate reference, and trabecular structure results were averaged over consecutive 4 mm thick image stacks (8 MRI images, 2 QCT images). For the TS scans the analysis region began 20 mm (radius) or 28 mm (tibia) from the endplate, and cortical results were averaged over 4 mm thick image stacks (2 MRI images, 2 QCT images). For MRI results were also calculated as an average over a single larger region: 16 mm thick starting 6 mm proximal from the endplate in the radius, and 12 mm thick starting 12 mm proximal from the endplate in the tibia. These were the largest regions that could be analyzed in all subjects.

### Statistics

Relationships between age, body mass index (BMI), QCT derived BMD, and MRI derived trabecular and cortical parameters were evaluated and compared using the Pearson product-moment correlation coefficient ( $r$ ). For the radius and tibia, MRI derived results (i) were given for four and three individual slices starting 6 and 12 mm from the distal endplate and (ii) were averaged over the entire scan volume (covering 16 and 12 mm). Only correlations reaching a significant  $p$ -value  $< 0.05$  are presented in the results section and will further be discussed.

## Results

### Correlations with age, BMI and weight

The most significant, yet moderate correlation was found between age and BMD of the spine with  $r = -0.52$  ( $p < 0.0001$ ), showing a decline in BMD with increasing age. At the hip, a lower, yet still significant correlation of  $r = -0.31$  ( $p < 0.05$ ) was found. Of all MRI derived parameters, the only significant, however low correlations ( $p < 0.05$ ) with age were found at the tibia for app. Tb.N ( $r = -0.36$ ) and app. Tb.Th ( $r = 0.35$ ), suggesting that a loss of trabeculae is compensated by an increase in trabecular thickness. Interestingly cortical parameters were not correlated with age.

BMI and weight dependent correlations with MRI and QCT measurements are listed in Table 1. At the weight bearing sites (tibia and calcaneus) MRI derived structure measures show significant relationships, with moderate  $r$ -values of 0.54 for app. Tb.N of the tibia ( $p < 0.05$ ). Overall the highest correlations are with weight rather than BMI.

### Interrelationship of BMD and MRI measurements

The intersite correlation between BMD values obtained at the spine and at the proximal femur reached  $r = 0.43$  ( $p < 0.002$ ). Correlations between spine BMD values and MRI derived values were significant at the radius and the tibia for Ct.Th measures ( $r_{\text{radius}} = 0.55$ ,  $p < 0.05$  and  $r_{\text{tibia}} = 0.67$ ,  $p < 0.0001$ ) and app. Tb.N ( $r_{\text{radius}} = 0.33$ ,  $p < 0.05$  and  $r_{\text{tibia}} = 0.35$ ,  $p < 0.05$ ).

Proximal femur BMD showed a correlation of  $r = 0.37$  ( $p < 0.05$ ) with radial app. Tb.N. At the site of the radius, with the only exception for app. Tb.Th, all trabecular structure parameters as assessed by MRI correlated well with BMD values from quantitative computed tomography at the same site (see Table 2).

### **Cortical and trabecular measurements, intrasite and intersite relationships**

In terms of intersite relationships, we found the highest and most significant correlations between cort.thick at the tibia and radius ( $r = 0.55$ ;  $p < 0.05$ ), between app. Tb.N at the tibia and calcaneus ( $r = 0.53$ ;  $p < 0.05$ ) (see Figure 2) and between app. Tb.Th at the tibia and radius ( $r = 0.48$ ;  $p < 0.05$ ). Furthermore, at the site of the radius there is an inverse correlation between cortical and trabecular parameters, showing increase in Ct.Th as app. BV/TV ( $r = -0.56$ ;  $p < 0.001$ ) and app. Tb.Th ( $r = -0.54$ ;  $p < 0.001$ ) decrease within the first 10 mm as seen in Table 3 and Figure 3.

### **Discussion**

In this study the feasibility of in vivo 3T MR imaging for the measurement of trabecular and cortical measures has been demonstrated. Furthermore the intrasite and intersite relationship of trabecular and cortical measures were investigated and correlations with volumetric BMD values as assessed by QCT were evaluated. The major findings are summarized below and will be discussed in detail separately.

#### **Feasible in vivo MR derived trabecular structure measure Tb.N**

Our results show that MRI derived app. Tb.N is the structure measure that gives the most significant correlations with age, BMD, BMI and weight. As expected, BMI and weight related correlations with app. Tb.N were highest in the load-bearing sites of the tibia and the calcaneus. Furthermore, both sites showed a significant intersite correlation of  $r = 0.53$  ( $p < 0.05$ ) for app. Tb.N. Furthermore, out of all MR derived measures obtained in this study app. Tb.N measured at the tibia showed significant correlation with age. At the radius moderate correlations between MRI derived app. Tb.N values and QCT derived BMD values were found. Correlations between spinal BMD and app. Tb.N were nearly equal in the tibia and the radius. The significant and often unique correlation of app. Tb.N with other measures of bone microarchitecture is in accordance with previously published in vitro and in vivo studies (19,22,26).

#### **Inverse relationship of cortical and trabecular measures at the radius**

We have assessed Ct.Th at the radius and the tibia and have observed - beyond the correlation with spinal BMD, and beyond a significant intersite relation - an inverse correlation with trabecular measures at the radius. This correlation shows that with increasing app. BV/TV and app. Tb.Th, Ct.Th decreases and vice versa. As, this is only a cross-sectional study on postmenopausal women one needs to carefully consider that it is difficult to differentiate this possible inverse - cortical and trabecular bone - interrelationship from effects of bone loss. Furthermore, when using a fixed distance to the endplate - for different sized bones - different relative distances between the imaged sites of each subject may bias the results. Overall, however, the fact remains that cortical and trabecular bone are interdependent compartments of one system, and bone physiology and bone pathology may not be explained adequately if morphological changes solely in one compartment are being investigated.

#### **Age dependent correlations with BMD and app. trabecular measures**

Age dependent correlations were, with the expectation of a moderate decrease in spinal BMD, low within our study. This is most likely caused by the fact that 49% of our study participants were between 50 and 59 years of age. Therefore, our data did not supply the necessary age

range to identify possible age dependent changes, considering that the 25% and 75% quartiles ranged from 56.42 and 67.34 years, covering only a difference of 10.34 years. Interestingly for MRI derived measures age showed no correlation with cortical thickness, whereas trabecular measures at the tibia revealed low yet significant correlations with age.

Until recently BMD measurements were the only approach to diagnose systemic bone diseases, however it has been demonstrated that by doing so only a small fraction of the dynamic bone homeostasis in osteoporosis is understood (27,28). Incorporation of trabecular bone distribution analysis with BMD measurements have resulted in significant improvements for the prediction of fracture risk and bone strength (14). It is to be expected that cortical bone structure analysis in combination with trabecular structure analysis will further improve research in this field.

## Conclusion

In conclusion our study has demonstrated that 3T MR imaging is a capable tool for the in vivo assessment of trabecular and cortical bone. 3T MRI derived measures show significant correlations with QCT derived BMD, suggesting that the two methodologies assess similar respectively complementary characteristics of bone. Furthermore MRI derived trabecular and cortical structure measures have been shown to have an intrasite dependent relationship. Overall in the future 3T MRI may be an alternative, non-ionizing tool for the assessment of fracture risk.

## References

1. Beck TJ, Ruff CB, Warden KE, Scott WW Jr, Rao GU. Predicting femoral neck strength from bone mineral data. A structural approach. *Invest Radiol* 1990;25(1):6–18. [PubMed: 2298552]
2. Bell GH, Cuthbertson DP, Orr J. Strength and size of bone in relation to calcium intake. *J Physiol* 1941;100(3):299–317. [PubMed: 16991528]
3. Hansson T, Roos B, Nachemson A. The bone mineral content and ultimate compressive strength of lumbar vertebrae. *Spine* 1980;5(1):46–55. [PubMed: 7361198]
4. Mosekilde L, Bentzen SM, Ortoft G, Jorgensen J. The predictive value of quantitative computed tomography for vertebral body compressive strength and ash density. *Bone* 1989;10(6):465–470. [PubMed: 2624829]
5. Osteoporosis prevention, diagnosis, and therapy. *Jama* 2001;285(6):785–795. [PubMed: 11176917]
6. Ammann P, Rizzoli R. Bone strength and its determinants. *Osteoporos Int* 2003;14 Suppl 3:S13–S18. [PubMed: 12730800]
7. Kanis JA, Borgstrom F, De Laet C, Johansson H, Johnell O, Jonsson B, Oden A, Zethraeus N, Pfleger B, Khaltav N. Assessment of fracture risk. *Osteoporos Int* 2005;16(6):581–589. [PubMed: 15616758]
8. Schuit SC, van der Klift M, Weel AE, de Laet CE, Burger H, Seeman E, Hofman A, Uitterlinden AG, van Leeuwen JP, Pols HA. Fracture incidence and association with bone mineral density in elderly men and women: the Rotterdam Study. *Bone* 2004;34(1):195–202. [PubMed: 14751578]
9. Fyhrie DP. Summary--Measuring "bone quality". *J Musculoskelet Neuronal Interact* 2005;5(4):318–320. [PubMed: 16340121]
10. Bouxsein ML. Bone quality: where do we go from here? *Osteoporos Int* 2003;14 Suppl 5:S118–S127. [PubMed: 14504716]
11. Seeman E, Delmas PD. Bone quality--the material and structural basis of bone strength and fragility. *N Engl J Med* 2006;354(21):2250–2261. [PubMed: 16723616]
12. Ladinsky GA, Vasilic B, Popescu AM, Wald M, Zemel BS, Snyder PJ, Loh L, Song HK, Saha PK, Wright AC, Wehrli FW. Trabecular structure quantified with the MRI-based virtual bone biopsy in postmenopausal women contributes to vertebral deformity burden independent of areal vertebral BMD. *J Bone Miner Res* 2008;23(1):64–74. [PubMed: 17784842]

13. Link TM, Saborowski, Kisters K, Kempkes M, Kosch M, Newitt D, Lu Y, Waldt S, Majumdar S. Changes in calcaneal trabecular bone structure assessed with high-resolution MR imaging in patients with kidney transplantation. *Osteoporos Int* 2002;13(2):119–129. [PubMed: 11905522]
14. Link TM, Vieth V, Langenberg R, Meier N, Lotter A, Newitt D, Majumdar S. Structure analysis of high resolution magnetic resonance imaging of the proximal femur: in vitro correlation with biomechanical strength and BMD. *Calcif Tissue Int* 2003;72(2):156–165. [PubMed: 12370799]
15. Majumdar S, Genant HK. Assessment of trabecular structure using high resolution magnetic resonance imaging. *Stud Health Technol Inform* 1997;4081–4096.
16. Majumdar S, Genant HK, Grampp S, Newitt DC, Truong VH, Lin JC, Mathur A. Correlation of trabecular bone structure with age, bone mineral density, and osteoporotic status: in vivo studies in the distal radius using high resolution magnetic resonance imaging. *J Bone Miner Res* 1997;12(1):111–118. [PubMed: 9240733]
17. Wehrli FW, Ford JC, Attie M, Kressel HY, Kaplan FS. Trabecular structure: preliminary application of MR interferometry. *Radiology* 1991;179(3):615–621. [PubMed: 2027962]
18. Wehrli FW, Ford JC, Haddad JG. Osteoporosis: clinical assessment with quantitative MR imaging in diagnosis. *Radiology* 1995;196(3):631–641. [PubMed: 7644622]
19. Krug R, Carballido-Gamio J, Burghardt AJ, Kazakia G, Hyun BH, Jobke B, Banerjee S, Huber M, Link TM, Majumdar S. Assessment of trabecular bone structure comparing magnetic resonance imaging at 3 Tesla with high-resolution peripheral quantitative computed tomography ex vivo and in vivo. *Osteoporos Int* 2008;19(5):653–661. [PubMed: 17992467]
20. MacNeil JA, Boyd SK. Accuracy of high-resolution peripheral quantitative computed tomography for measurement of bone quality. *Med Eng Phys* 2007;29(10):1096–1105. [PubMed: 17229586]
21. Phan CM, Matsuura M, Bauer JS, Dunn TC, Newitt D, Lochmueller EM, Eckstein F, Majumdar S, Link TM. Trabecular bone structure of the calcaneus: comparison of MR imaging at 3.0 and 1.5 T with micro-CT as the standard of reference. *Radiology* 2006;239(2):488–496. [PubMed: 16569786]
22. Sell CA, Masi JN, Burghardt A, Newitt D, Link TM, Majumdar S. Quantification of trabecular bone structure using magnetic resonance imaging at 3 Tesla--calibration studies using microcomputed tomography as a standard of reference. *Calcif Tissue Int* 2005;76(5):355–364. [PubMed: 15868282]
23. Laib A, Newitt DC, Lu Y, Majumdar S. New model-independent measures of trabecular bone structure applied to in vivo high-resolution MR images. *Osteoporos Int* 2002;13(2):130–136. [PubMed: 11905523]
24. Parfitt AM, Drezner MK, Glorieux FH, Kanis JA, Malluche H, Meunier PJ, Ott SM, Recker RR. Bone histomorphometry: standardization of nomenclature, symbols, and units. Report of the ASBMR Histomorphometry Nomenclature Committee. *J Bone Miner Res* 1987;2(6):595–610. [PubMed: 3455637]
25. Newitt DC, van Rietbergen B, Majumdar S. Processing and analysis of in vivo high-resolution MR images of trabecular bone for longitudinal studies: reproducibility of structural measures and micro-finite element analysis derived mechanical properties. *Osteoporos Int* 2002;13(4):278–287. [PubMed: 12030542]
26. Kazakia GJ, Hyun B, Burghardt AJ, Krug R, Newitt DC, de Papp AE, Link TM, Majumdar S. In vivo determination of bone structure in postmenopausal women: a comparison of HR-pQCT and high-field MR imaging. *J Bone Miner Res* 2008;23(4):463–474. [PubMed: 18052756]
27. Cummings SR. Are patients with hip fractures more osteoporotic? Review of the evidence. *Am J Med* 1985;78(3):487–494. [PubMed: 3976707]
28. Ott SM. When bone mass fails to predict bone failure. *Calcif Tissue Int* 1993;53 Suppl 1:S7–S13. [PubMed: 8275383]

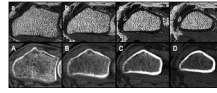


**Figure 1.**

Matched cross sectional images of the distal radius obtained with 3T MR imaging (top row) and volumetric QCT (bottom row) at different slice positions as compared to the endplate (a/ A - 6 mm proximal to the endplate; b/B - 10 mm proximal to the endplate; c/C - 14 mm proximal to the endplate; d/D 18 mm proximal to the endplate). For each slice position, the mean values of the trabecular structure parameters (+/- standard deviation) are given in Table 3a.

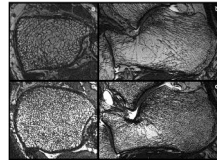


**Figure 2.**

3T MR images of the tibia (a, c) and calcaneus (b, d) from two different subjects. Note the sparse trabecular bone structure of the top images (a, b) as compared to the dense trabecular bone structure depicted in the bottom images (c,d).

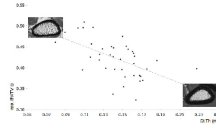


**Figure 3.** Correlation of  $r = -0.56$  ( $p < 0.001$ ) between app. BV/TV measures obtained 6 mm proximal to the endplate and Ct.Th measures. The top left image shows an example of a distal radius with high app. BV/TV values as compared to the example shown in the bottom right image.

**Table 1**

Correlations between MRI parameters and spinal BMD vs. BMI and weight.

		<b>BMI</b>	<b>Weight</b>
Radius	app. BV/TV	n.s.	n.s.
	app. Tb.N	n.s.	n.s.
	app. Tb.Th	n.s.	n.s.
	app. Tb.Sp	n.s.	n.s.
	Ct.Th	0.38*	0.43*
Tibia	app. BV/TV	n.s.	n.s.
	app. Tb.N	0.40*	0.54*
	app. Tb.Th	n.s.	-0.38*
	app. Tb.Sp	-0.34*	-0.40*
	Ct.Th	n.s.	n.s.
Calcaneus	app. BV/TV	0.30*	0.41*
	app. Tb.N	0.32*	0.37*
	app. Tb.Th	n.s.	n.s.
	app. Tb.Sp	-0.35*	-0.43*
Spine	BMD	0.39*	0.41*
Femur	BMD	n.s.	n.s.

correlation coefficient (r);

\*\*  
p < 0.0001;\*  
p < 0.05;

n.s. non significant (p &gt; 0.05)

**Table 2**

Correlation between MRI derived structural parameters acquired at the radius and BMD values assessed at the same site.

MRI derived structural parameters	trabecular BMD by QCT
app. BV/TV	0.58**
app. Tb.N	0.59**
app. Tb.Th	0.39*
app. Tb.Sp	-0.50*

correlation coefficient (r);

\*\*  
p < 0.0001;

\*  
p < 0.05

**Table 3**

Correlation between MRI derived BV/TV and app. Tb.Th values as compared to Ct.Th measures at the radius.

	6 mm distance to endplate		10 mm distance to endplate	
	app. BV/TV	app. Tb.Th	app. BV/TV	app. Tb.Th
Ct.Th	-0.56**	-0.54**	-0.36*	-0.41*

correlation coefficient (r);

\*\*  
p < 0.001;

\*  
p < 0.05